STRUCTURAL CONTROL AND HEALTH MONITORING
Struct. Control Health Monit. 2009; **16**:441–459
Published online 28 April 2008 in Wiley InterScience
(www.interscience.wiley.com). DOI: 10.1002/stc.262

Embeddable corrosion rate-measuring sensor for assessing the corrosion risk of steel in concrete structures

R. Vedalakshmi*,†, H. Dolli and N. Palaniswamy

Corrosion Protection Division, Central Electrochemical Research Institute, Karaikudi 630 006, Tamil Nadu, India

SUMMARY

New and rehabilitated concrete structures \need assessment of corrosion rate (CR) of rebars more precisely to ensure efficiency of protection against corrosion. For assessing the corrosion status, different sensors have been developed to reduce the risk of undetected corrosion problems. An embeddable CR-measuring sensor is embedded either closer to the rod during the construction of a new structure or in drilled holes in old structures so as to generate reliable data. In the present paper, the accuracy in predicting the corrosion current (I_{corr}) by embeddable sensor was assessed by comparing with other conventional electrode arrangements. I_{corr} was assessed under passive and active conditions of rebar. The presence of a cross bar and the effect of cover on I_{corr} were also studied. Using linear polarization resistance (LPR) technique and electrochemical impedance spectroscopic (EIS) technique, the CR was determined and compared with the weight-loss method. Results concluded that by using electrochemical impedance technique, developed embeddable sensor is able to predict the CR very close to the CR determined from gravimetric method. The deviation from an ideal linear curve and the higher interfacial capacitance of steel in concrete caused the LPR method to underestimate the CR of rebar. The presence of the cross bar increases the I_{corr} of the main bar by 4 times in a passive state of the rebar and it has no effect if the rebar is in an active state. The embedded sensor, though having smaller counter electrode (CE), polarizes the rebar up to 2 times the length of CE under both active and passive states. Copyright © 2008 John Wiley & Sons, Ltd.

KEY WORDS: embeddable sensor; surface-mounted sensor; polarization resistance; linear polarization resistance (LPR) technique; electrochemical impedance spectroscopic (EIS) technique; corrosion rate; weight-loss method

1. INTRODUCTION

Corrosion of reinforcement embedded in either reinforced or prestressed concrete structure is the main cause of deterioration. Maintenance and restoration of these structures as well as

*Correspondence to: R. Vedalakshmi, Corrosion Protection Division, Central Electrochemical Research Institute, Karaikudi 630 006, Tamil Nadu, India.
†E-mail: corrveda@yahoo.co.in

Received 28 January 2007
Revised 17 January 2008
Accepted 26 February 2008

Copyright © 2008 John Wiley & Sons, Ltd.

quality control requires reliable and non-destructive techniques that can detect corrosion status of a rebar at an early stage. Nowadays in new and rehabilitated concrete structures, the rate of corrosion of the rebar with time has been done to ensure long lifetime requirements to estimate the efficiency of protection of the new/repaired concrete against corrosion. The techniques used for assessing the condition of the rebar are potential and resistivity, which measure only corrosion state of the rebar. Whereas the electrochemical techniques such as linear polarization resistance (LPR) technique, electrochemical impedance spectroscopic (EIS) technique and galvanostatic pulse technique (GPT) measure the corrosion rate (CR) of the rebar. All the above techniques can be used either in isolation or in combination to identify the 'highly corroding' or 'non-corroding' state of the rebar embedded in the concrete structure. In all these techniques, usually a surface-mounted sensor (SMS), which may be either a 'guard ring' or a 'small/large counter electrode (CE)' than the rebar length, has been used in the field and laboratory conditions, respectively [1–3]. The former is used for an unknown steel area, whereas the latter is convenient for a known steel area. Nowadays, different embeddable sensors have been developed to monitor the corrosion of the reinforcement to reduce the risk of undetected corrosion problems. These sensors are permanent corrosion monitoring system, which are embedded in concrete during the construction of new structures or into drilled holes of existing structures [4–8].

The method of monitoring using embeddable sensor is very effective in the following situations: (i) in highest point of portal frame in framed structures, columns and beams located at elevated height, (ii) in bridge structure one traffic lane has to be closed for a certain time, (iii) in concrete surface coated with an insulating paint and (iv) in carbonated concrete because of the reduction in pH of the alkaline pore solution, it offers more resistance to the concrete, which leads to the erroneous measurement [9]. Embeddable sensor is a viable method in such a situation where the conventional surface-mounted probe arrangement cannot be used. Changes in the rebar with time at same locations even by remote monitoring are possible by embedded sensors to assess the service life of the structure and it is an additional advantage over the SMS.

In concrete structures, there are two types of embeddable sensors that have been normally used since 1990. One is embeddable reference electrode, which measures the potential of the rebar, and the other one is embeddable CR-measuring sensor, which measures the corrosion current. The drawback of the potential sensor is that the potential of the reference electrode is affected by the changes in the contents of moisture, oxygen, chloride level and pH of the concrete more directly than the conventional surface-mounted reference electrodes [10]. For measuring the corrosion current, different sensor configurations are developed. Schiessel and Raupach developed a sensor called 'anode ladder' or 'the expansion ring system', which measures the resistance of the concrete, potential and current of the rebar based on the principle of macro cell corrosion current [5,6]. The anode ladder consists of arrays of mild steel and stainless steel bars. Mild steel bars are embedded at discrete points in the cover zone. Macro cell current flow was measured between each mild steel anode and a stainless steel cathode. The anodic current flow through the element is used to follow the depassivation front through the cover zone. The sensor developed by Swedish FORCE Institute detects the initiation of corrosion by a sudden rise in the anodic current [7]. The sensor based on the measurement of electrical conductivity to study the properties of cover zone concrete has been used and the conductivity was correlated with probable CR of the rebar [11,12]. The sensor comprises 10 electrode pairs mounted on a small plexiglas former. Each electrode comprises a 1.2 mm diameter stainless steel pin, which was sleeved to expose a 5 mm tip. The pairs of electrodes were

Copyright © 2008 John Wiley & Sons, Ltd.

DOI: 10.1002/stc

then arranged vertically at 5 mm intervals thus enabling electrical measurements to be taken at 10 discrete points over a depth of 50 mm. Using impedance analyzer at a frequency of 1 kHz at 10 mV signal amplitude, the resistance of the concrete was measured and correlated with the probable CR values. An attempt was also made using steel/copper-coupled and steel/stainless–steel-coupled galvanic sensor in the concrete, the galvanic current output was related with the real corrosion damage of the reinforcing steel [13,14]. In the electrode arrangements, electrodes that are 12 mm in diameter and 45 mm in length were mounted on an epoxy resin, which insulated them from each other. Using the zero resistance ammeter, the galvanic current output was measured. The increase in the current output indicates the onset of the corrosion of the rebar. All these sensors described above predict the probability of the corrosion and do not give the CR of the rebar directly.

Embeddable CR-measuring sensor is another system, essentially consisting of a reference electrode, a CE (graphite or stainless steel) and a separately embedded mild steel working electrode, which should be representative of the actual rebar of the known area, which is also widely used. It measures the potential, the polarization resistance (R_p) of the rebar and the resistance of the concrete (R_c) [7,15,16]. For existing structures, prepotted linear polarization sensors by isolating a piece of the rebar were also installed at representative locations to evaluate the effectiveness of the repaired concrete [15]. Isolating a piece of the rebar enables to have a controlled measurement area without resorting to guard rings or separately embedded working electrodes.

The method of approach of the present investigation is to study the accuracy in assessing the polarization resistance (R_p) of the rebar using the developed embeddable CR-measuring sensor and compare it with the other electrode configurations normally used for measuring the corrosion of the rebar under the laboratory condition. Among the other electrode configurations, one is the SMS, which is widely used under both laboratory and field conditions and consists of a saturated calomel electrode as a reference electrode and stainless steel as a CE. The length of the CE is larger than the exposed length of the rebar. In another electrode arrangement, two rebars as similar to the working electrode are kept adjacent to both sides of the rebar and act as CEs [3,16], which are normally used in the laboratory condition for achieving uniform distribution of the current on the rebar. I_{corr} was determined using two electrochemical techniques such as LPR method and EIS method under passive and active states of the rebar. The CR determined by embedded sensor was compared with the rate determined by the other electrode arrangements and gravimetric method.

2. EXPERIMENTAL PROGRAM

2.1. Fabrication of embeddable CR-measuring sensor

The embeddable CR-measuring sensor (ES) consists of a solid-state metal oxide as a reference electrode and a stainless electrode as a CE. Stainless steel sheet of the size 4.5 cm in length is fixed in a rectangular PVC gadget and a metal oxide reference electrode was centrally embedded. The electrical leads were taken from both the electrodes through the PVC gadget as shown in Figure 1. The patented and fabricated reference electrode is based on the solid-state metal oxide that offers stable reference potential suitable for permanent installation in the concrete environment [17]. The reversible potential of the metal oxide reference electrode is +450 mV. The fabricated reference electrode was evaluated in the concrete medium as per the standard test

Copyright © 2008 John Wiley & Sons, Ltd.

DOI: 10.1002/stc

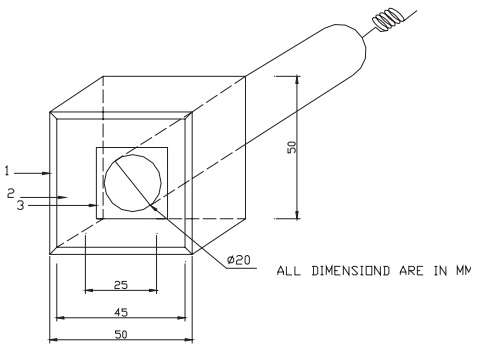

1.PVC Cell

2.Stainless steel counter Electrode

3.Reference Electrode

Figure 1. Schematic diagram of the embeddable sensor.

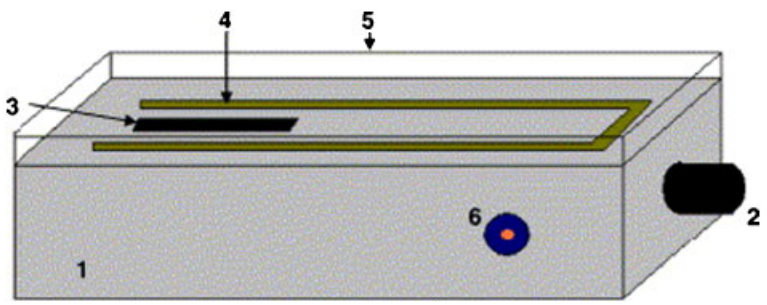

Figure 2. Schematic diagram of surface-mounted sensor (as reproduced from Reference [34]): (1) PVC; (2) reference electrode; (3) hole for wetted sponge; (4) SS counter electrode; (5) wetted sponge; and (6) electrical connection for counter electrode.

procedure and was found to have stable, reliable and reproducible electrode potential during the standardization process [18]. The SMS consists of a stainless steel sheet of 13 cm length, in which saturated calomel electrode is centrally embedded in the PVC sheet as shown in Figure 2.

2.2. Materials

Ordinary Portland cement conforming to I.S:81129:2003 [equivalent to ASTM-Type-I cement] was used and the composition was (wt%) SiO_2: 20–21%; Al_2O_3: 5.2–5.6%; Fe_2O_3: 4.2–4.8%; CaO: 62–63%; MgO: 0.5–0.7%; SO_3: 2.4–2.8%; LOI: 1.5–2.5% and others 0.1%. The well-graded river sand and good-quality crushed blue granite aggregates conforming to IS 383:2004 were used as fine and coarse aggregates, respectively. Thermomechanically treated bars (TMT) of 10 mm diameter were used. Potable water was used for casting the concrete.

Copyright © 2008 John Wiley & Sons, Ltd.

DOI: 10.1002/stc

2.3. Specimen preparation

Cubical concrete specimens of 150 mm size were cast using the mix proportion of 1:2.19:3.73 with a w/c ratio of 0.5. The characteristic compressive strength of the concrete at 28 days was 25 MPa. Bars of 10 mm diameter and 100 mm long were embedded at a cover of 25 mm. Both top and bottom ends of the rods were sealed using the epoxy compound by leaving an exposed length of 8.5 cm. Electrical leads were taken from the bars and sealed. During concreting, the embeddable sensor assembly was embedded at a distance of 10 mm from the rebar as shown in Figure 3(A). When making measurements using SMS, the assembly as shown in Figure 2 was kept on the wetted sponge on the concrete surface as shown in Figure 3(B). In another electrode arrangement, during concreting two rebars of similar dimension as the main rebar have been kept on both sides of the rebar (adjacent rebars as CE) and embeddable metal oxide reference electrode was placed at the center of these two adjacent electrodes as shown in Figure 3(C).

2.3.1. Effect of interference of cross bar. The presence of cross bar on the CR measurement of the main bar was studied using ES and SMS. For analyzing this, another bar of the similar dimension as the main bar was tied at the center of the main bar in perpendicular direction as shown in Figure 3(D). The additional bar has been treated as a cross bar and this rebar assembly was kept at a 25 mm cover in 150 mm cubical concrete specimens.

2.3.2. Effect of cover. The availability of moisture, oxygen and chloride presence in the cover concrete on the CR measurement using SMS and ES is also studied. For this, the rebar was embedded at a cover of 50 mm in the 150 mm size cubical concrete specimens. ES was embedded at a distance of 10 mm from the rebar as shown in Figure 3(E).

After 28 days of water curing, all the concrete specimens were air cured for 7 days under laboratory condition.

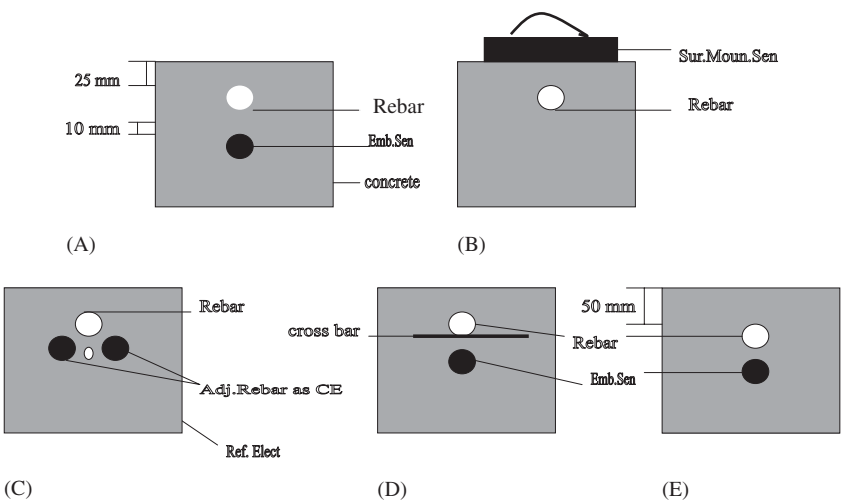

Figure 3. Electrodes arrangements: (A) embedded sensor (rebar at 25 mm cover); (B) surface-mounted sensor; (C) adjacent rebars as counter electrode; (D) presence of cross bar; and (E) embedded sensor (rebar at 50 mm cover).

Copyright © 2008 John Wiley & Sons, Ltd.

DOI: 10.1002/stc

3. METHOD OF MEASUREMENT AND EXPOSURE

3.1. Passive state of rebar

The method of measurement using different electrode configurations is shown in Figure 3(A)–(E). After allowing 7 days of air curing, the R_p value of the rebar under passive state was measured using LPR and EIS techniques. Both measurements were carried out on the same concrete specimen with an interval of 24 h. The EIS measurement was followed by an LPR measurement. In the case of rebar with the cross bar, measurement was carried out only on the main bar. In the EIS measurement, using the electrochemical impedance analyzer (EC&G instruments) model no. 6310, frequency range between 100 kHz and 10 mHz with an AC amplitude of 20 mV was applied. The impedance values at each frequency were plotted on the Nyquist plot. From the Nyquist plot, using the software 'z view', the concrete resistance (R_c) and polarization resistance (R_p) were determined by extrapolating the high-frequency arc (100 kHz–100 Hz) and low-frequency arc (100 Hz–10 mHz), respectively.

In the LPR measurement, using the potentiostat model no. 1285 (Solartron), the rebar was polarized ± 20 mV from the open circuit potential at a scan rate of 0.1667 mV/s. The change in potential (E) and the change in current (I) were plotted. Using the software 'corrview', from the slope of the curve, the R_p value (which is inclusive of R_c) was calculated. The IR compensation arisen from the high resistance of the concrete has not been compensated during the measurement, the R_c value as determined from the EIS method has been deducted from the R_p value and true R_p value was calculated. Measurements were made on duplicate specimens and the average R_p value has been reported.

From the R_p values determined by both the techniques by assuming B as 26 mV, the I_{corr} was calculated using the Stern–Geary relation [19] as follows:

$$\mathbf{I}_{corr} = \frac{B}{R_p} \tag{1}$$

where B is the Stern–Geary constant, 26 mV for both active and passive states of the rebar; R_p is the polarization resistance, $\Omega\,cm^2$ and I_{corr} is the corrosion current, $\mu A/cm^2$. From the $I_{corr,}$ the CR of the rebar was calculated using the following formula:

$$\text{Corrosion rate, mmpy} = 0.0116 \times \mathbf{I}_{corr} \tag{2}$$

Measurements were carried out on the rebar having cross bar at its center and the rebar at 50 mm cover. In the case of rebar with cross bar, measurements were made on the main bar only.

3.2. Active state of the rebar

By conducting an accelerated corrosion test, active state of the rebar was induced. A PVC bund of 5 cm depth was fixed on the one side of the specimen from which the cover was measured. About 3% NaCl solution was ponded. Corrosion was induced by applying a current density of $350\,\mu A/cm^2$ anodically using the stainless steel as a CE. The current was applied for a period of 5 days. After 5 days of the application of the current, the specimens were allowed to depolarize for 5 days to reach the steady-state condition. Then LPR and EIS measurements as explained in Section 3.1 were carried out using both sensor configurations.

Copyright © 2008 John Wiley & Sons, Ltd.

DOI: 10.1002/stc

3.3. Comparison of CR: electrochemical measurements vs weight-loss method

The reliability in assessing the CR under the active condition using ES and SMS was compared with the CR by the weight-loss measurement. For this, before embedding the rebar, the initial weight (W_1) of the rebar was taken. To have a sufficient mass loss of the rebar at 50 mm cover, an anodic current of 350 $\mu A/cm^2$ was applied to the rebar for 21 days. The experiment was conducted with the rebar embedded at both the covers. After 21 days of the application of the current, the specimens were allowed to depolarize for 5 days to reach the steady-state condition. After making the electrochemical measurement, the specimens were broken open and the rebars were taken out. Then they were pickled in the inhibited hydrochloric acid as specified in ASTM G1 [20]; the final weight (W_2) was recorded. From the weight loss, the CR was calculated using the following formula:

$$\text{Corrosion rate in mmpy} = \frac{87.6 \times w}{DAT} \tag{3}$$

where w is the loss in weight, mg; D is the density of iron, gm/cm^3; A is the area, cm^2; T is the time, h.

CR determined from the weight-loss method was compared with the rate determined by the LPR and EIS techniques.

3.4. Measurement of the CR of the rebar in the rehabilitated portal-framed structure using ES

Sixteen numbers of embedded sensors (as described in the text) were embedded in the rehabilitated portal-framed reinforced concrete structure situated in the Nuclear Fuel complex, Hyderabad, India. For the long-term corrosion monitoring of the rehabilitated cover concrete, the sensors were embedded in columns, beams and purlins. The structure was rehabilitated with the self-compacting concrete with additional protective measures such as by coating to rebars as well as coating to entire concrete surface. The additional rebars provided in the cover concrete and the exposed area of the rebars in the old concrete were coated with polymer coating. As the concrete surface was coated with an insulating paint, to monitor the rebars at highest locations in purlins, embedded sensors are more appropriate than SMSs. The compressive strength of the cover concrete is 30 MPa and the rebars were embedded at 40 mm cover at all locations. Before concreting, the sensors were tied along with the main bar at a distance of 10–15 mm as shown in Figure 4. Because of coated rebars, the R_p value of the rebar was determined by the EIS technique using the ACM (Advanced Corrosion Monitoring, U.K.) field machine. Because of the smaller CE used in ES and as the rebars are in passive state, the length of the spread out of the current signal on the rebar than the CE length was determined by conducting two R_p measurements by assuming the polarized length of the rebar is equal to the CE length (L_{c1}) and 3 times of CE length (L_{c2}), respectively. From the two R_p values, the i_{c1} and i_{c2} were calculated. Using the following formulae, the length up to which the current spreads outside the length of CE (L_{crit}) and the total polarized length were calculated:

$$L_{crit} = \frac{L_{c1} \times L_{c2}(i_{c2} - i_{c1})}{2(i_{c1} \times L_{c1} - i_{c2} \times L_{c2})} \tag{4}$$

$$\text{Total polarized length} = L_{c1} + 2L_{crit} \tag{5}$$

The L_{crit} was determined in columns and beams and the average value was reported. After conducting the EIS measurement at various locations, the R_p value was calculated from the

Copyright © 2008 John Wiley & Sons, Ltd.

DOI: 10.1002/stc

Figure 4. Embedded sensor in beam.

Nyquist plot. From the R_p value, the i_{corr} was calculated using the total polarized length. The measurements were carried out initially at the end of the construction as well as after 1 year. The I_{corr} obtained at few representative locations are given in Table VI.

4. RESULTS AND DISCUSSION

4.1. Passive state of the rebar

4.1.1. Impedance technique. Figure 5 compares the Nyquist plot of the rebar embedded in the concrete under the passive state using all electrode configurations. From the plot it can be seen that there are two arcs that are present: one at high-frequency region and another at low-frequency region. The high-frequency arc (100 kHz–100 Hz) is contributed by the solid phase of the hydrated cement products present in the concrete and free ions in the pore solution. The low-frequency arc (100 Hz–10 mHz) is contributed by the protective passive layer (lime-rich product) formed on the rebar surface. Using ES, the rebar at 50 mm cover clearly shows the capacitive nature because of the presence of the Warburgh impedance and it is mainly by the diffusion-controlled reaction. Whereas this is not clearly observed when the rebar is at 25 mm cover. According to the Nyquist plot obtained the assumed equivalent circuit consists of two time constants, which is given in Figure 6. The non-uniform distribution of the current on the main bar by the presence of cross bar made the arc more deformed.

When comparing the I_{corr} (Table I), I_{corr} measured by the ES as well as the adjacent rebar, as CE is more or less same, which is 0.2212 and 0.2349 $\mu A/cm^2$, respectively. This indicates that similar to adjacent rebars, ES uniformly distribute the current to the whole length of the rebar exposed. In ES, the length of the CE is 4.5 cm, which is smaller than the length of the rebar exposed, but it polarizes the rebar to the exposed length of 8.5 cm. Escalante *et al.* reported similar observation that the smaller CE polarizes the steel surface to twice the area represented by the electrode (CE) length [21]. I_{corr} of the main bar in the presence of the cross bar is 0.9722 $\mu A/cm^2$, which is 4 times higher than that of the rebar without the cross bar. Non-uniform distribution of the current on the main bar by the presence of cross bar causes higher I_{corr}. Gonzalez *et al.* [16] also reported a similar observation on the interconnected rebar

Copyright © 2008 John Wiley & Sons, Ltd.

DOI: 10.1002/stc

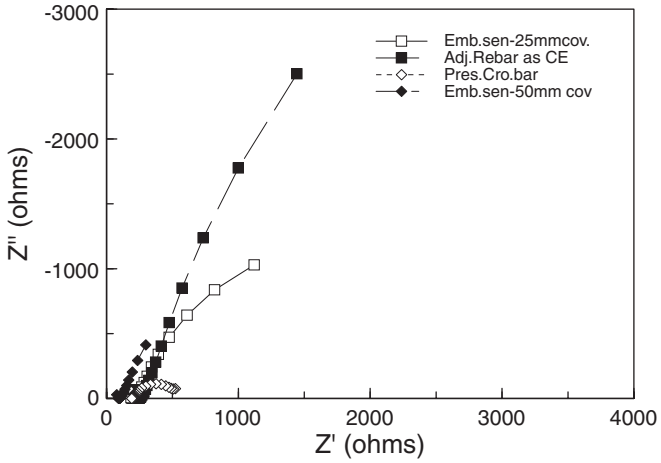

Figure 5. The Nyquist plot of rebar embedded in concrete using embedded sensor—under passive state of rebar.

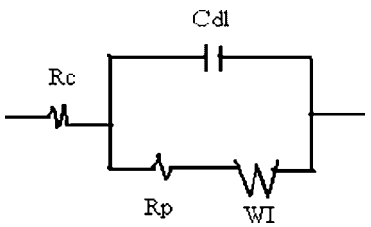

Figure 6. Equivalent circuit of rebar under passive state: R_c, concrete resistance; Cdl, double layer capacitance; R_p/R_{ct}, charge transfer resistance of rebar; and WI, Warburg impedance.

Table I. I_{corr} using the EIS technique: embedded sensor *vs* surface-mounted sensor (passive state of rebar).

	25 mm cover			50 mm cover		
Type of electrode arrangement	R_c (Ω)	R_p (Ω)	I_{corr} (μA/cm^2)	R_c (Ω)	R_p (Ω)	I_{corr} (μA/cm^2)
Embedded sensor	292	4404	0.2212	266	8687	0.1121
Surface-mounted sensor	317	3764	0.2588	581	7427	0.1312
Adjacent rebar as CE	159	4147	0.2349	—	—	—
Presence of cross bar						
ES	205	501	0.9722	—	—	—
SMS	370	537	0.9070	—	—	—

network using the small CE. Gonzalez *et al*. reported that the I_{corr} determined using the small CE kept on the top surface of the slab is 100 times higher than that of the I_{corr} determined using the adjacent rebar as CE in the cement mortar slab containing no chloride, i.e. under passive state of rebar. The higher I_{corr} by SMS indicates the non-uniform distribution of current on the

Copyright © 2008 John Wiley & Sons, Ltd.

DOI: 10.1002/stc

main bar by the presence of interconnected bars. In the present study as the rebar contains only one cross bar, 4 times increase in I_{corr} was obtained. At 50 mm cover, ES measures the lowest I_{corr} of 0.1121 $\mu A/cm^2$. Videm and Myrdal [22] reported that the passivation current density of the iron immersed in the alkaline solution is less than 0.2 $\mu A/cm^2$ and observed that it was independent of potential and pH. The current density obtained is $\leqslant 0.2\,\mu A/cm^2$ as reported in the literature and shows that the rebar is in perfect passive condition.

From Table I, it is seen that I_{corr} predicted by SMS at 25 mm cover of concrete is 0.2588 $\mu A/cm^2$ and it is 0.1312 $\mu A/cm^2$ at 50 mm cover. The I_{corr} values measured by SMS are slightly higher than the value predicted by ES. In estimating the concrete resistance, significant difference is observed between the two sensors. The values of R_c measured by SMS are higher than that measured by ES. For example, R_c measured by SMS at 25 mm cover is 317 Ω and it is 518 Ω at 50 mm cover. Whereas in the case of ES, R_c is 292 Ω at 25 mm cover and it is 266 Ω at 50 mm cover. SMS measures the R_c, which depending upon the cover of the concrete whereas ES measures R_c only at 10 mm from the rebar irrespective of the cover of the concrete. This is clearly indicated by the observed value of R_c that is more or less equal at both the covers.

In EIS technique, the resistance of the concrete was excluded from the R_p value determined by both SMS and ES and due to this not much difference is observed in the measured I_{corr} value.

4.1.2. Linear polarization technique. As shown in Figure 7, the slope of the *E vs I* curve at 50 mm cover is less than at 25 mm cover and does not change when using the adjacent rebar as CE. From the slope of the curve, apparent R_p value was determined. The R_c value determined from the impedance method has been deducted from the R_p value and true R_p was arrived. If this is not done, the R_p value will be overestimated and the calculated I_{corr} will be smaller than the actual value [23]. From Table II, it can be seen that I_{corr} measured using ES and adjacent rebar as CE are 0.2080 and 0.2036 $\mu A/cm^2$, respectively. However, the presence of the cross bar causes 8 times higher I_{corr} value than that of the main bar without the cross bar. At 50 mm cover, ES measures I_{corr} value of 0.2858 $\mu A/cm^2$, which is 2.5 times higher than the value determined by EIS. The measured I_{corr} under passive state of the rebar using both the sensors is around 0.2 $\mu A/cm^2$.

From the results it is inferred that at passive state of the rebar up to a 25 mm cover, the I_{corr} determined using both sensors by EIS and LPR is more or less the same. However, at 50 mm cover, I_{corr} by SMS is higher. The higher interfacial capacitance of the rebar in concrete may overshadow the Faraday current under normal scan rate [24,25] and this may increase the I_{corr} to a value of 0.3040 $\mu A/cm^2$, which is 2.3 times higher than the I_{corr} predicted by ES. As reported in the literature, the sweep rate used in the LPR method also influences the I_{corr} value. Gonzalez *et al*. [26] recommended the sweep rates between 0.04 and 0.17 mV/s for potentio-dynamic polarization to achieve a steady-state condition. However, for passive steel much lower sweep rates of 0.04 mV/s can be appropriate because the attainment of the steady state is extremely slow [27]. However, slower sweep rate may cause changes in the rebar. In the present study a sweep rate of 0.1667 mV/s has been used and sweep rate less than this may change the electrode surface because of longer polarization time. The sweep rate should be long enough to allow the transitory component to disappear and short enough to avoid changes in the rebar. Hence, a scan rate of 0.1667 mV/s is more appropriate and does not probably affect the I_{corr} value determined by the LPR technique.

Copyright © 2008 John Wiley & Sons, Ltd.

DOI: 10.1002/stc

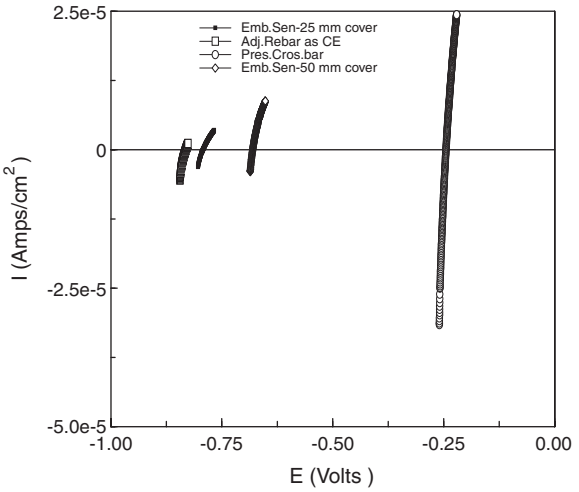

Figure 7. Linear polarization behavior of rebar embedded in concrete using embedded sensor—under passive state of rebar.

Table II. I_{corr} using the LPR technique: embedded sensor *vs* surface-mounted sensor (passive state of rebar).

	25 mm cover			50 mm cover		
Type of electrode arrangement	R_c (Ω)	R_p (Ω)	I_{corr} (μA/cm^2)	R_c (Ω)	R_p (Ω)	I_{corr} (μA/cm^2)
Embedded sensor	292	4684	0.2080	266	3408	0.2858
Surface-mounted sensor	317	4281	0.2276	581	3204	0.3040
Adjacent rebar as CE	159	4784	0.2036	—	—	—
Presence of cross bar						
ES	205	589	1.6535	—	—	—
SMS	370	912	1.0681			

From the discussion it can be observed that the cover of concrete is more than 25 mm, it influenced the I_{corr} measured by the LPR method, whereas I_{corr} by the EIS method is not much affected by the cover of the concrete.

4.2. Active state of the rebar

4.2.1. Impedance technique. After 5 days of the application of the current, the rebar gets corroded (active state). Under this active state of the rebar, the impedance behavior of the rebar using ES is given in Figure 8. From the figure it can be seen that the diameter of the high-frequency arc is decreased by the permeation of moisture and chloride ions. The low-frequency arc is much flatter and deformed, which indicates that the rebar gets uniformly corroded. Now the reaction is under charge transfer control. However, at 50 mm cover depth, as there is no deformed semi-circle the rebar is still under diffusion-controlled reaction. The slope of the

Copyright © 2008 John Wiley & Sons, Ltd.

DOI: 10.1002/stc

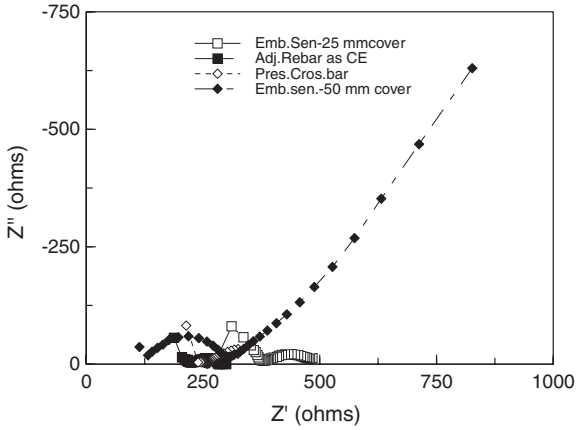

Figure 8. The Nyquist plot of rebar embedded in concrete using embedded sensor—under active state of rebar.

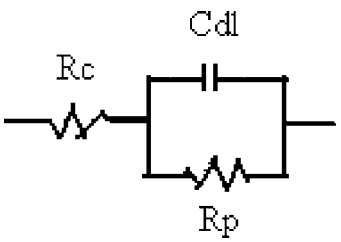

Figure 9. Equivalent circuit of rebar under active state.

low-frequency arc is nearly −1, which indicates that the corrosion may be initiated on the rebar. The pattern of the curve using adjacent rebar as CE is same as ES. The presence of the cross bar does not distort very much the curve obtained by ES. The assumed equivalent circuit according to the behavior of the Nyquist curve is given in Figure 9.

Table III compares the R_p and R_c values of the rebar using ES and SMS. It shows that I_{corr} of the rebar using ES and adjacent rebar as CE are 8.1179 and 7.0083 $\mu A/cm^2$, respectively. This clearly indicates that the ES polarizes the rebar throughout the exposed length. It is also seen that the presence of the cross bar does not affect the I_{corr} of the main bar and the I_{corr} value is 8.1179 $\mu A/cm^2$, which is equal to the value measured using ES. At 50 mm cover, the I_{corr} is 0.2372 $\mu A/cm^2$, which is 40 times less than the rebar at 25 mm cover. Reduced permeation of chloride ions and resistance offered by the higher cover reduced the I_{corr} at 50 mm cover.

The I_{corr} of the rebar measured using SMS is slightly less than the I_{corr} measured using ES both at 25 and 50 mm covers. I_{corr} of the main bar in the presence of the cross bar using SMS is 6.0506 $\mu A/cm^2$, which is almost equal to I_{corr} of 6.3670 $\mu A/cm^2$ without the cross bar. From this, it is inferred that the presence of the cross bar does not affect the I_{corr} of the main bar when it is in the active state.

Copyright © 2008 John Wiley & Sons, Ltd.

DOI: 10.1002/stc

Table III. I_{corr} using the EIS technique: embedded sensor *vs* surface-mounted sensor (active state of rebar).

	25 mm cover			50 mm cover		
Type of electrode arrangement	R_c (Ω)	R_p (Ω)	I_{corr} (μA/cm^2)	R_c (Ω)	R_p (Ω)	I_{corr} (μA/cm^2)
Embedded sensor	89	120	8.1179	182	4107	0.2372
Surface-mounted sensor	133	153	6.3670	218	5135	0.1897
Adjacent rebar as CE	81	139	7.0083	—	—	—
Presence of cross bar						
ES	23	120	8.1179	—	—	—
SMS	83	161	6.0506			

The concrete resistance measured by SMS is higher. It is 133 at 25 mm cover and 218 Ω at 50 mm cover concrete, respectively. Comparing with the R_c value at passive condition, i.e. before chloride ponding, the R_c value decreases after exposure to chloride. Permeation of chloride ions causes the reduction in the resistance of the concrete At 50 mm cover of concrete, the resistance value is 182 Ω using ES and it is 218 Ω by SMS. As the difference between the R_c value measured by SMS and ES is less, it indicates that not much chloride has permeated during the exposure period through the 50 mm cover of concrete. However, at 25 mm cover of concrete, the R_c value measured by SMS is 133 Ω, which is 1.5 higher than the R_c measured using ES. In addition to the presence of chloride, moisture available in the cover concrete at the time of measurement also influences the measured R_c values using SMS.

From the above discussion, it is inferred that when measuring I_{corr} using EIS, it is more or less same as measure ES and using the adjacent rebar as CE. Unlike in passive state, under active state the presence of the cross bar does not alter the I_{corr} measured on the main bar and thus the current is confined to the main bar only. Because the spread out of the current signal larger than the length of CE is negligible on actively corroding rebars. Elsener *et al*. [28] reported that under the active condition, the current spreads out less than 0.5 cm than the length of CE land and even a guard ring is not necessary. However, under passive state of the rebar, the current spreads not only on the main bar but also on the interconnected bar. Hence, the length of the rebar polarized could not be predicted in the presence of the cross bar and higher I_{corr} was obtained.

4.2.2. Linear polarization technique. Figure 10 compares the polarization behavior of the rebar using ES under the active state. The slope of the curve is lesser than that obtained at the passive state of the rebar. As shown in Table IV, the I_{corr} values predicted by ES and adjacent rebar as CE are 3.690 and 3.8504 μA/cm^2, respectively. The I_{corr} of the main bar in the presence of the cross bar is 3.5553 μA/cm^2 and shows that it does not alter the I_{corr} of the main bar. I_{corr} at 50 mm cover is 0.3864 μA/cm^2, which is 7 times less than that of the I_{corr} at 25 mm cover. However, I_{corr} determined by SMS is less than the value by ES in all electrode configurations except at 50 mm cover. The presence of the cross bar reduces the I_{corr} of the main bar by 3 times when measured using SMS.

The I_{corr} predicted by SMS under both active and passive states is less than that predicted by ES. Either the presence of moisture or the lack of oxygen in the cover concrete influences the I_{corr} measured by SMS whereas ES embedded at 10–15 mm from the rebar, the presence of

Copyright © 2008 John Wiley & Sons, Ltd.

DOI: 10.1002/stc

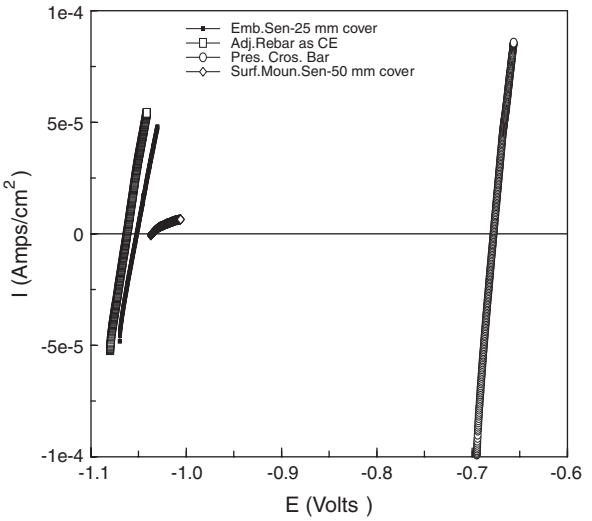

Figure 10. Linear polarization behavior of rebar embedded in concrete using embedded sensor—under active state of rebar.

Table IV. I_{corr} using the LPR technique: embedded sensor *vs* surface-mounted sensor (active state of rebar).

	25 mm cover			50 mm cover		
Type of electrode arrangement	R_c (Ω)	R_p (Ω)	I_{corr} (μA/cm^2)	R_c (Ω)	R_p (Ω)	I_{corr} (μA/cm^2)
Embedded sensor	89	264	3.6900	182	221	0.3864
Surface-mounted sensor	133	285	3.4181	218	2081	0.4681
Adjacent rebar as CE	81	253	3.8504	—	—	—
Presence of cross bar						
ES	23	274	3.5553	—	—	—
SMS	83	532	1.831			

moisture and oxygen at very lower cover did not influence the measured I_{corr} value and thus predicted the I_{corr} very close to the actual value. This is one of the advantages of ES over conventional SMS for long-term monitoring of the rebar corrosion in new and old concrete structures.

4.3. Potential vs *time: comparison between ES and SMS*

4.3.1. Passive state. Figure 11 compares the potential of rebar measured under passive and active conditions using the embedded reference electrode and the reference electrode kept at the surface over a period of 11 months. Initially there is not much difference between them. However, at the end of 30 days, the potential of rebar when it is in passive condition is −75 mV using ES and it is −194 mV by SMS. After 11 months of exposure, a potential difference of 87 mV was observed between them. Formation of passive layer on the rebar by the hydrated

Copyright © 2008 John Wiley & Sons, Ltd.

DOI: 10.1002/stc

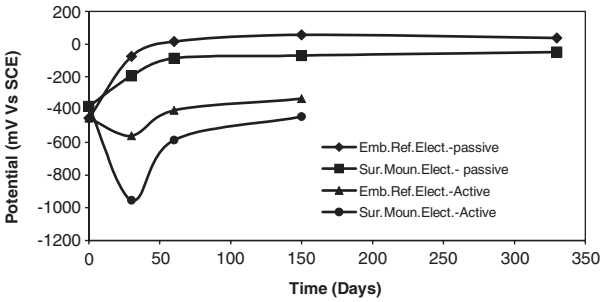

Figure 11. Comparison of potential-time behavior using embedded sensor *vs* surface-mounted sensor—under passive and active state of rebar.

cement products, which grows in thickness with time, shifts the potential value to more +ve direction. Videm observed a potential difference of 120 mV between embedded and surface measured electrodes when measured in Gimsoystraumen Bridge, U.S.A. [29]. The liquid junction potential variations in pH and oxygen concentration in the cover concrete caused more negative potential by keeping reference electrode on the concrete surface than the actual value measured by embedding the reference electrode very near to the rebar [30,31]. It is clearly observed that the embedded reference electrode eliminates the errors introduced by surface electrodes and indicates the actual potential of the rebar.

4.3.2. Active state. Under active condition of rebar, the experiment was conducted over a period of 150 days and the potential has been compared only up to 150 days. From Figure 11, it can be seen that initially the potential of rebar is −453 mV using ES and it is −381 mV by SMS. The potential difference between them was 72 mV. Potential measured by both the sensors decreases with time and reaches −332, −442 mV at the end of 150 days. A difference in 110 mV was observed between them. Because of the non-uniform corrosion and the presence of corrosion macro cells on the rebar, the potential measurement near the rebar causes more −ve value when the potential was measured on the concrete surface [31,32]. Results clearly indicate that embedded reference electrode near the rebar measures the actual potential of the rebar under both active and passive states of rebar and the errors introduced by the cover concrete are greatly minimized.

4.4. Comparison of CR: gravimetric method vs *electrochemical techniques*

Table V compares the CR by gravimetric method with the rate determined by electrochemical techniques. It can be seen that the LPR technique underestimates the CR measured by both ES and SMS than that with the CR determined by weight-loss method. Whereas using the EIS technique, the ES predicted the CR very close to the CR by weight-loss method. Only 15% of variation was observed between them. However, the LPR method variation is 72%, which is quite high. The adjacent rebar as CE also predicts the CR very close to the CR determined by weight-loss method. Only 18% of variation was observed between them. It is also seen that using ES, the EIS method predicts the CR of main bar more precisely than the other methods and was not affected by the presence of cross bar. Sathyanarayanan *et al.* [33] also

Copyright © 2008 John Wiley & Sons, Ltd.

DOI: 10.1002/stc

Table V. Comparison of corrosion rate: electrochemical techniques *vs* weight-loss method.

Type of electrode arrangement	Corrosion rate by weight-loss method (mmpy)	Corrosion rate by embedded.sensor (mmpy)		Corrosion rate by surface-mounted sensor (mmpy)	
		EIS	LPR	EIS	LPR
Embeddedsensor—25 mm cover	0.1724	0.1468	0.0474	0.1270	0.0316
Embeddedsensor—50 mm cover	0.0423	0.0684	0.0521	0.0290	0.0173
Adjacent rebar as CE	0.1922	0.1569	0.1000	0.1000	0.0850
Presence of cross bar	0.1068	0.1056	0.0554	0.0611	0.0301

reported similar observation by comparing the CR by the LPR technique with weight-loss method and found that in the presence of chlorides, LPR underestimates the CR by one order of magnitude than by the gravimetric method. At 50 mm cover, the ES measures the CR of rebar as 0.0684 and 0.0521 mmpy in EIS and LPR method, respectively, whereas by weight-loss method it is 0.0423 mmpy. CR predicted using both techniques by SMS is lower than by weight-loss method.

Deviation of the linear polarization curves from the ideal linear shape causes the underestimation of CR by the LPR method [29,31]. In addition to this, the capacitive charging current arises from the presence of capacitance at the steel-concrete interface was found to be more than the Faraday current. Owing to these reasons the LPR method is found to be less suitable for the determination of CR. However, determination of R_p using EIS is least influenced by the polarization-induced charges of the steel surface; hence, it predicts the CR more precisely than the LPR method. From these results it is also inferred that the R_p value is between 117 and 231 $k\Omega\,cm^2$ if the rebar is in the passive state and it is less than 5 $k\Omega\,cm^2$ if the rebar is in the active state. Sagues and Sorn and Oshiro also reported similar observation for passive and active conditions of rebar [34,35]. Now relatively cheap and portable equipment for field measurement has recently become commercially available. Therefore, in future though time consuming, EIS technique will be much more used in the field for measuring accurate CR of rebar using both embedded sensors and SMSs.

4.5. CR of the rebar in the rehabilitated portal-framed structure

The average L_{crit} measured by ES at the site is found to be 1.5 cm and total polarized length is 7.5 cm, which is equal to 1.67 times of length of CE. The use of coated rebar and high-strength concrete in the structure is a probable reason for the reduction of polarized length to 1.67 times from 2 times as observed in the laboratory investigation. The Nyquist plot at one of the locations (i.e. in beam) is given in Figure 12. From the figure it can be seen that there are three arcs that are present distinctly in the plot. Compared with Figure 5, the additional arc obtained in the plot is due to the presence of barrier coating at the steel–concrete interface.

From Table VI, it can be seen that the CR values are in the range of 0.00028–0.0033 mmpy. As the structure is rehabilitated recently and the use of coated rebars helps to obtain the negligible CR values in the structure.

Copyright © 2008 John Wiley & Sons, Ltd.

DOI: 10.1002/stc

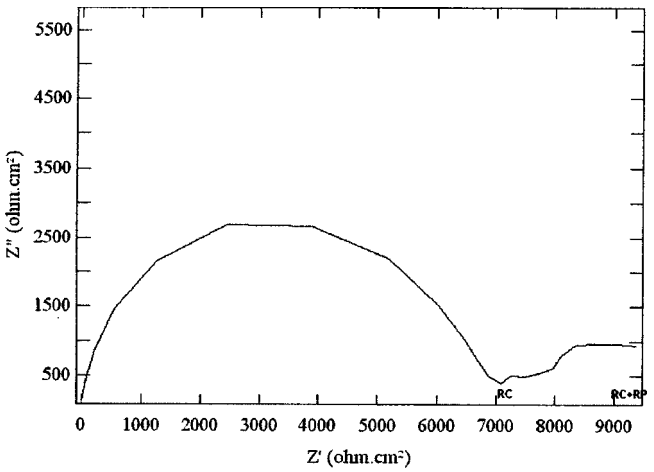

Figure 12. The Nyquist plot of coated rebar measured using ES in beam.

Table VI. Corrosion rate using ES in portal-framed structure.

	Corrosion rate (mmpy)							
Measurement made	Columns			Beams		Purlins		
Locations	1	2	3	1	2	1	2	3
Initial	0.0008	0.0016	0.0009	0.0005	0.0033	0.0008	0.0019	0.0023
After 1 year	0.0004	0.00195	0.0015	0.0018	0.00076	0.00095	0.00028	0.00087

5. CONCLUSIONS

1. Using the EIS technique, the developed embeddable CR-measuring sensor is able to predict the CR that is more or less equal to CR determined by the gravimetric method under both passive and active states of the rebar. The embedded sensor predicts the CR very close to the value determined by adjacent rebar as CE, indicating that ES distributes the current uniformly throughout the length of the exposed rebar. Though the length of the CE in the sensor assembly is less than the exposed length of the rebar it is able to polarize the rebar up to 8.5 cm length. The confinement of electrical signal is 2 times of the length of the CE under passive and active conditions of rebar.
2. Under active state of rebar, the LPR method underestimates the CR. The deviation of the LPR curve from an ideal linearity and the higher interfacial capacitance of steel in concrete are the probable reasons.
3. The presence of cross bar increases the I_{corr} of main bar by 4 times if the rebar is in passive state and its presence has no effect if the rebar is in the active state. The errors introduced in measuring CR using SMS can be minimized by using ES and it may be an alternate solution for measuring the CR of rebar very close to the actual value.

Copyright © 2008 John Wiley & Sons, Ltd.

DOI: 10.1002/stc

4. The data collected from the rehabilitated portal-framed structure reveal that the current spreads out 1.6 times of the CE length.
5. Embeddable sensor can predict the CR precisely under both EIS and LPR techniques. The advantage of EIS over the LPR method is by observing separate arcs for each time constant it is able to separate the capacitance of the rebar and resistance of the concrete from the R_p value. Although EIS technique is time consuming, it will be much more useful in the field and is suitable for both embedded sensors and SMSs in predicting the CR.

REFERENCES

1. Sehgal A, Kho YT, Osseo-Asare K, Pickering HW. Comparison of corrosion rate measuring devices for determining corrosion rate of steel in concrete. *Corrosion* 1992; **48**(10):871–880.
2. Feliu J, Sabol S, Pickering HW, Sehgal A, Osseo-Asarea K, Cady PD. Electrochemical measurements on concrete bridges for evaluation of reinforcement corrosion rates. *Corrosion* 1993; **49**(7):601–613.
3. Gonzalez JA, Cobo A, Gonzalez MN, Feliu S. On-site determination of corrosion rate in reinforced concrete structures by use of galvanostatic pulses. *Corrosion Science* 2001; **43**(4):611–625.
4. Schiessel P, Raupach M. Monitoring system for the corrosion risk of steel in concrete structures. *Concrete International* 1992; (**6**):52–55.
5. Bjegovic D, Mikulic D, Sekulic D. Non-destructive corrosion rate monitoring for reinforced concrete structures, 2000. www.ndt.net/article/wcndt00/paper.idn642/idn642.htm.
6. Bjegovic D, Miksic B, Stehly R. Test protocols for migrating corrosion inhibitors (MCI) in reinforced concrete. *Emerging Trends in Corrosion Control-evaluation*, *Monitoring*, *Solutions*, vol. 1. India Akademia Books International and NACE International, India Section: New Delhi, 1999; 3–8.
7. Nagayama M. MCI 2020 long term protection of rebar in concrete. *Final Report*, General Building Corporation of Japan, October 1999.
8. McCarter WJ, Vennesland O. Sensor systems for use in reinforced concrete structures. *Construction and Building Materials* 2004; **18**:351–358.
9. Arup H, Sorenson B. A new embeddable reference electrode for use in concrete structures. *Proceedings of Corrosion/92. Paper No. 208*. NACE International: Houston, U.S.A., 1992.
10. Castro P, Sagues AA, Moreno EI. Characterization of activated titanium solid reference electrodes for corrosion testing of steel in concrete. *Corrosion* 1996; **58**(8):609–617.
11. McCarter WJ, Chrisp TM, Starrs G, Basheer PAM, Blewett J. Field monitoring of electrical conductivity of cover-zone concrete. *Cement & Concrete Composites* 2005; **27**:809–817.
12. McCarter WJ, Chrisp TM, Butler A, Basheer PAM. Near surface sensors for condition monitoring of cover-zone concrete. *Construction and Building Materials* 2001; **15**:115–124.
13. Yoo JH, Park ZT, Kim JG, Chung L. Development of a galvanic sensor system for detecting the corrosion damage of the steel embedded in concrete structures: part I. Laboratory tests to correlate galvanic current with actual damage. *Cement and Concrete Research* 2003; **33**:2057–2062.
14. Park ZT, Choi Y, Seok CY, Kim GJ, Chung L. Development of a galvanic sensor system for detecting the corrosion damage of the steel embedded in concrete structures: part 2. Laboratory electrochemical testing of sensors in concrete. *Cement and Concrete Research* 2005; **35**:1814–1819.
15. Broomfield JP, Kevin Davies, Karel Hladky. The use of permanent corrosion monitoring in new and existing reinforced concrete structures. *Cement & Concrete Composites* 2002; **24**:27–34.
16. Gonzalez JA, Miranda JM, Feliu S. Considerations on reproducibility of potential and corrosion rate measurements in reinforced concrete. *Corrosion Science* 2004; **46**(10):1:2467–1:2474.
17. Dolli H, Muralidharan VS, Rengaswamy NS. Reliability evaluation of embeddable reference electrode for use in reinforced concrete structures. *Bulletin of Electrochemistry* 2003; **19**(1):212–217.
18. Dolli H, Muralidharan VS, Rengaswamy NS. Improvements in or relating to the development of an embeddable reference electrode for multifarious applications. Indian Patent No.: 315DIL/2002, 2002.
19. Stern M, Geary AL. Electrochemical polarization: I. A theoretical analysis of the shape of polarization curves. *Journal of the Electrochemical Society* 1957; **104**(1):56–63.
20. ASTM G1-90. Standard practice for preparing, cleaning and evaluating corrosion test specimens. *ASTM Standards*, vol. 03.02, 2000; 9.
21. Escalante E, Whitemton E, Qiu F. Measuring the rate of corrosion of steel in concrete. *Final Report, NBS-NBSIR 86–3456*, October 1986; 1.

Copyright © 2008 John Wiley & Sons, Ltd.

DOI: 10.1002/stc

22. Videm K, Myrdal R. The electrochemical behaviour of steel in concrete and how to evaluate the corrosion rate. *Proceedings of Corrosion/96. Paper No. 96348*. NACE International: Houston, U.S.A., 1996.
23. Andrade C, Castelo V, Alonso C, Gonzalez JA. In *Corrosion Effect of Stray Currents and the Techniques for Evaluating Corrosion of Rebars in Concrete. ASTM STP-906*. Chaker V (ed.). ASTM—Special Technical Publication: Philadelphia, PA, 1986; 43.
24. Sagues AA, Kranc SC. Scan rate effects on the determination of polarization diagrams; application to steel in concrete. *Proceedings of First NACE Latin American Region Corrosion Congress and First Venezuelan Corrosion Congress. Paper No. 94043*. NACE International: Houston, U.S.A., 1994.
25. Kouril MP, Novak P, Bojko M. Limitations of the linear polarization method to determine stainless corrosion rate in concrete environment. *Cement and Concrete Composites* 2006; **28**:220–225.
26. Gonzalez JA, Molina A, Eskudero MC, Andrade C. Errors in the electrochemical evaluation of very small corrosion rates—I. Polarisation resistance method applied to corrosion of steel in concrete. *Corrosion Science* 1995; **25**:917–923.
27. Mansfeld F, Kendig M. Concerning the choice of scan rate in polarization measurements. *Corrosion* 1981; **37**:545–552.
28. Elsener B, Klinghoffer O, Frolund T, Rislund F, Schiegg Y, Bohni H. Assessment of reinforcement corrosion by means of galvanostatic pulse technique. *Proceedings of International Conference on Repair of Concrete Structures*, Svolvaer, Norway, 1997.
29. Videm K. The reliability of electrochemical techniques for assessing corrosion of steel in concrete. *Proceedings of Corrosion/98. Paper No. 98749*. NACE International: Houston, U.S.A., 1998.
30. Myrdal R. Phenomena that disturb the measurements in concrete. *Proceedings of Corrosion/96. Paper No. 96339*. NACE International: Houston, U.S.A., 1998.
31. Myrdal R. Potential gradients in concrete caused by charge separations in a complex electrolyte. *Proceedings of Corrosion/97. Paper No. 97278*. NACE International: Houston, U.S.A., 1997.
32. Mansfeld F, Kendig M. Concerning the choice of scan rate in polarization measurements. *Corrosion* 1981; **37**:545–552.
33. Sathyanarayanan S, Natrajan P, Saravanan K, Srinivasan S, Venkatachari G. Corrosion monitoring of steel in concrete by galvanostatic pulse technique. *Cement Concrete Composites* 2006; **28**:630–637.
34. Sagues AA. Corrosion measurement techniques for steel in concrete. *Corrosion/93. Paper No. 353*. NACE International: Houston, U.S.A., 1993.
35. Sorn V, Oshiro T. Performance of fly ash concretes in accelerated and natural chloride exposure regime. *Proceedings of 7th CANMET/ACI International Conference on Fly Ash, Silica Fume, Slag and Natural Pozzolans in Concrete, SP-199*, vol. I. ACI: Detroit, U.S.A., 2001; 185–204.

Copyright © 2008 John Wiley & Sons, Ltd.

DOI: 10.1002/stc